PAPER

Check for updates

Understanding the mechanism of the competitive adsorption in 8-methylquinoline hydrogenation over a Ru catalyst†

Yuan Dong,[a] Haoming Zhao,[a] Zhenjie Liu,[a] Ming Yang, [ID] *[ab] Zhenlin Zhang,[a] Ting Zhu[a] and Hansong Cheng*[a]

The competitive adsorption of 8-methylquinoline (**8-MQL**) and partially hydrogenated product, **4H-8-MQL**, was studied by performing a combination of experiments and first-principles calculations over a selected Ru catalyst. A series of hydrogenation reactions were conducted with **8-MQL** and **4H-8-MQL** as initial reactants, respectively. **8-MQL** exhibits stronger adsorption on catalyst surface active sites compared with **4H-8-MQL** and the massive adsorption of **8-MQL** hampers the further adsorption of **4H-8-MQL**. The effects of temperature, pressure and solvent on the selectivity in **8-MQL** hydrogenation were investigated as well. Full hydrogenation of **8-MQL** to **10H-8-MQL** was achieved within 120 min when the catalyst dosage increased from 5 wt% to 7 wt% under 160 °C and a hydrogen pressure of 7 MPa. The electronic charge of the N-heteroatom in **8-MQL** and **4H-8-MQL** was analyzed and the adsorption geometries of **8-MQL** and **4H-8-MQL** on the Ru(001) surface were optimized by DFT calculations to explain the competitive adsorption behaviors of **8-MQL** and **4H-8-MQL**.

Introduction

The direct hydrogenation of quinoline (QL) and its derivatives is considerably interesting for the industrial synthesis of a variety of petrochemicals, pharmaceuticals and fine chemicals.[1–3] Both partially hydrogenated products and fully hydrogenated products are valuable chemicals as well as liquid organic hydrogen storage materials.[4–8] Therefore, the role of reaction parameters in the selectivity of QLs hydrogenation is widely investigated for obtaining the required product.[9–13] Two hydrogenated intermediates, 1,2,3,4-4H-QL and 5,6,7,8-4H-QL, were generated along with the completely hydrogenated product, 10H-QL. It is found that the selectivity to 4H-QL or 10H-QL is affected dramatically by the catalysts and solvents used in QL hydrogenation.[14–16] Heterogeneous catalysts based on Rh,[3,17] Pd,[18,19] Ru[20,21] and Pt[22] were successfully used in selective hydrogenation of QLs to 4H-QLs. Yu et al. reported that 99.8% 4H-QL can be achieved over prepared Ru/OMNC (ordered mesoporous N-doped carbon) catalyst with EtOH as solvent under 40 °C and 1 MPa H₂.[21] Pt/CeO₂ was found to be highly efficient and chemoselective hydrogenation of QL into 4H-QL at 60 °C, which was attributed to the metal-support interaction between Pt and

basic CeO₂.[23] 98% 4H-QL was achieved over cobalt-based catalyst under 120 °C and 2 MPa H₂ with toluene as the solvent reported by Chen et al.[24] Higher hydrogenation rates of 4H-QLs were observed in aqueous solvent compared to that in an aprotic and apolar solvent using supported Pd and Ru catalyst.[10,18] Ionic liquid stabilized Ni and Pt nanoparticles were also selected as highly efficient catalysts in chemoselective hydrogenation of QLs.[25–27] In addition, homogeneous catalysts based on Ir,[28] Ru,[29,30] Mo,[31] Co[32,33] were proposed to hydrogenate quinolines selectively as well.

The further hydrogenation, 4H-QL to 10H-QL, was proved to be more difficult, which requires longer reaction time and harsher conditions ($T > 100$ °C, $P > 5$ MPa).[34,35] Only 0.6% 10H-QL was converted from 4H-QL after QL hydrogenation for 14 h over supported Ru at 150 °C and 5 MPa.[36] This was explained mostly by the irreversible adsorption of QL and/or 4H-QL on the catalyst surface, also called catalyst poisoning, leading to the hydrogenation stops after 4H-QL production.[37,38] Actually, some effective methods have been developed to realize selective hydrogenation by adjusting the adsorption behaviors of QL and 4H-QL. Addition of a Lewis base[39] or introduction of aprotic solvent such as n-hexane[40,41] to the reaction mixture was in favor of 10H-QL formation. Fan et al. reported an excellent catalyst for complete hydrogenation of QL, Rh/AlO(OH).[40] They proposed that the hydrogen bond formed between hydroxyl group of Rh/AlO(OH) and the aromatic cycle of 4H-QL promotes 10H-QL production. However, the particular research on the competitive adsorption behaviors of QLs and 4H-QLs have been rarely reported.

[a]Sustainable Energy Laboratory, Faculty of Materials Science and Chemistry, China University of Geosciences, Wuhan 430074, P. R. China. E-mail: yangming8180@gmail.com; chenghs@cug.edu.cn

[b]Zhejiang Institute, China University of Geosciences, Hangzhou 311305, P. R. China

† Electronic supplementary information (ESI) available. See DOI: 10.1039/d0ra01277g

In the present work, 8-methylquinoline (**8-MQL**) hydrogenation was investigated over commercial Ru/Al$_2$O$_3$ under designed conditions to elaborate the competitive adsorption between **8-MQL** and **4H-8-MQL**. A series of hydrogenation reactions were conducted with **8-MQL** and **4H-8-MQL** as initial reactants, respectively. It is found that the adsorption of **4H-8-MQL** on Ru/Al$_2$O$_3$ is weaker than that of **8-MQL** and **4H-8-MQL** is not responsible for the catalyst poisoning. The role of reaction parameters including temperature, pressure and solvent in **8-MQL** hydrogenation was studied in detail. In addition, the adsorption geometries of **8-MQL** and **4H-8-MQL** was optimized by DFT calculations and the corresponding adsorption energies were also compared.

Results and discussion

Hydrogenation of 8-MQL to form 4H-8-MQL

The standard hydrogenation conditions designed in the present work were: 0.2 g Ru/Al$_2$O$_3$ catalyst, 4 g **8-MQL**, 40 ml dioxane with the hydrogen pressure of 7 MPa and reaction temperature range of 160–180 °C. As shown in Fig. 1, almost 100% of **8-MQL** was converted to form **4H-8-MQL** under designed conditions detected by GCMS. The structure of the produced **4H-8-MQL** was determined to be 1,2,3,4-**4H-8-MQL** by ^{1}H NMR, implying that **8-MQL** hydrogenation firstly occurred in N-heterocycle as a result of the strong interaction between N atom and the catalyst active site. The NMR spectrum was presented in Fig. S1.† Increase temperature from 160 °C to 180 °C, the conversion rate of **8-MQL** was accelerated obviously whereas only a trace of fully hydrogenated products (yield < 1%), **10H-8-MQL**, was detected. Similarly, hydrogenation of QL to produce 10H-QL catalyzed by supported noble metal catalyst was also found to be very difficult, which was roughly attributed to the strong adsorption of QL and/or 4H-QL on the effective active sites.[23,40]

Hydrogenation of 4H-8-MQL to form 10H-8-MQL

The **4H-8-MQL** produced from **8-MQL** hydrogenation was used as reactant after distillation. The standard conditions in this experiment were: 0.2 g Ru/Al$_2$O$_3$, 4 g **4H-8-MQL**, 40 ml dioxane, 7 MPa hydrogen pressure and 160 °C reaction temperature. Fig. 2 demonstrates that the fully hydrogenated product, **10H-8-MQL** was obtained as soon as the reaction started. Moreover, the same catalyst was reused 3 times for **4H-8-MQL** hydrogenation. No significant decrease in hydrogenation rate was observed, indicating that Ru/Al$_2$O$_3$ is highly active to catalyze **4H-8-MQL** to form **10H-8-MQL** and that **4H-8-MQL** is not responsible for poisoning the catalyst surface active sites.

The reaction pathway for **8-MQL** and **4H-8-MQL** hydrogenation has been described in Scheme 1. Both of process (1) and (3) can be realized successfully. In contrast, the process (2) of **10H-8-MQL** formation in hydrogenation of **8-MQL** was rarely observed even when the reaction temperature was increased to 180 °C. By comparing process (1) and process (3), the conversion rate of **4H-8-MQL** was slower than that of **8-MQL** under the same reaction conditions. 85% of **8-MQL** can be converted to **4H-8-MQL** within 120 min at 160 °C and 7 MPa, while only 30% of **4H-8-MQL** was consumed to produce **10H-8-MQL**.

It is widely acknowledgement that adsorption on the catalyst active sites was an essential prerequisite for hydrogenation reaction to occur. Therefore, we speculated that **8-MQL** were more easily adsorbed on the active sites such as metal surface and acid sites than that of **4H-8-MQL**, leading to the desorption of **4H-8-MQL** and thus **10H-8-MQL** was rarely produced. The re-exposure of active sites was in favor of the continuous hydrogenation of **8-MQL**. This hypothesis was proved by adding a new portion of **8-MQL** after the previous **8-MQL** was almost totally converted to **4H-8-MQL**. The results showed that a further 50% conversion of the fresh **8-MQL** to **4H-8-MQL** can be obtained within 60 min. The weaker interaction of **4H-8-MQL** with surface active sites compared with that of **8-MQL** probably results in the difficulty in effective adsorption on active sites and low conversion rate for its further hydrogenation.

Hydrogenation of 8-MQL to form 10H-8-MQL

In the view of the previous studies, it is can be deduced that **4H-8-MQL** could probably be further hydrogenated to form **10H-8-**
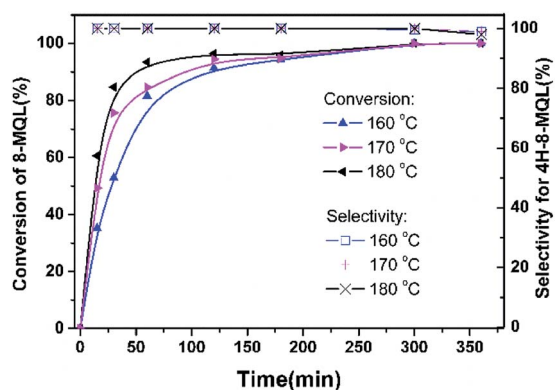

Fig. 1 Hydrogenation of **8-MQL** at different temperatures over Ru/Al$_2$O$_3$ with catalyst dosage proportion of 5 wt% and hydrogen pressure of 7 MPa.
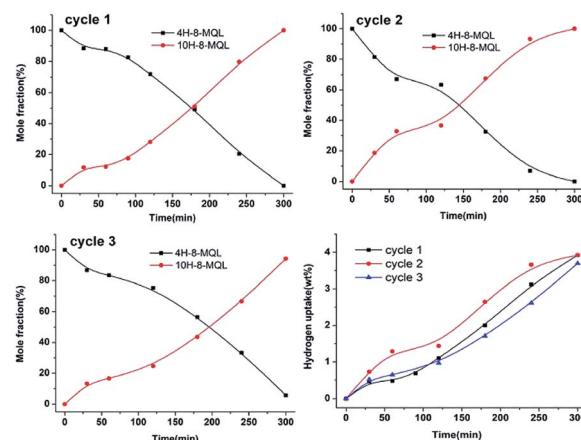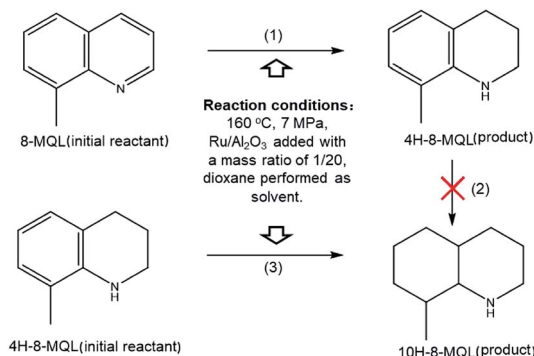

Fig. 2 Hydrogenation of **4H-8-MQL** at 160 °C and 7 MPa with the same Ru/Al$_2$O$_3$ catalyst for 3 cycles.
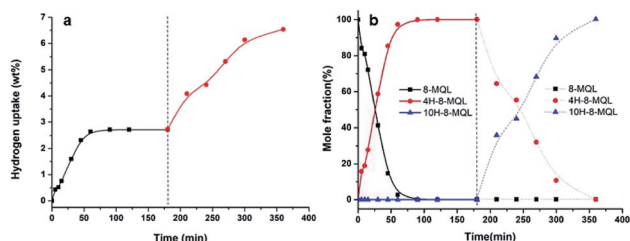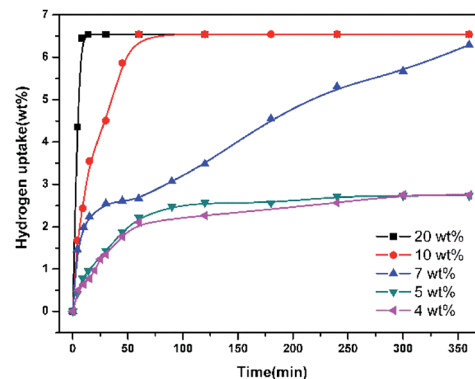
Scheme 1 Hydrogenation pathway of **8-MQL** and **4H-8-MQL** at 160 °C and 7 MPa over Ru/Al$_2$O$_3$ catalyst with the dosage proportion of 5 wt%.

Fig. 4 Influence of catalyst dosage proportions on the hydrogenation of **8-MQL**. General reaction conditions: 4 g **8-MQL**, 40 ml dioxane as solvents, 160 °C, 7 MPa H$_2$.

MQL if there were enough effective active sites in **8-MQL** hydrogenation. Hence, another dose of fresh catalyst was introduced to the reaction mixture after complete **8-MQL** was converted to **4H-8-MQL**. The result has been presented in Fig. 3. **4H-8-MQL** was consumed rapidly as soon as the reaction started. Finally, **10H-8-MQL** with a yield of 100% was obtained. The results confirmed that the absence of **10H-8-MQL** in **8-MQL** hydrogenation is attributed to the catalyst poisoning caused by strong adsorption of **8-MQL** occurred in the process of **8-MQL** to **4H-8-MQL**. However, it is believed that Ru/Al$_2$O$_3$ is essentially capable of hydrogenation of **8-MQL** to form **10H-8-MQL**. This assumption was confirmed by adding different dosage proportion of Ru/Al$_2$O$_3$ in the range of 4 wt% to 20 wt% for **8-MQL** hydrogenation at 160 °C and 7 MPa. The hydrogen uptake curves *vs.* reaction time have been displayed in Fig. 4.

Table 1 summarizes the conversion and selectivity during **8-MQL** hydrogenation with catalysts introduced in different mass ratios. At the catalyst dosage proportion of 4 wt% and 5 wt%, the rapid consumed **8-MQL** was totally converted to **4H-8-MQL** in the first 120 min. Keeping the reactions for another 4 hours, still almost no **10H-8-MQL** was observed. Differently, **4H-8-MQL** was gradually converted to form **10H-8-MQL** after 30 min when the dosage proportion of Ru/Al$_2$O$_3$ was increased from 5 wt% to 7 wt%. Further increase the dosage proportion to 20 wt%, 100% of **10H-8-MQL** can be produced within 15 min. This can be

attributed to the more effective active sites given by the catalyst with higher mass ratio, which makes more opportunities for successful adsorption of **4H-8-MQL** on catalyst surface and benefits the further hydrogenation of **4H-8-MQL**.

Fig. 5a and b display the hydrogen uptake curves *vs.* time of **8-MQL** hydrogenation at different temperatures and pressures with the catalyst dosage proportion of 10 wt%, respectively. It is found that complete **10H-8-MQL** can be produced within 60 min at 160 °C and 7 MPa. The apparent active energy of **8-MQL** consumption was derived to be 75.2 kJ mol^{-1} based on the first order reaction kinetics model. The products concentration distribution curves of **8-MQL** hydrogenation at different temperatures and pressures have been presented in Fig. S2 and S3,† respectively. The consumption of **8-MQL** gives rise to a fast accumulation of **4H-8-MQL**. Subsequently, the conversion from **4H-8-MQL** to **10H-8-MQL** starts. Particularly worth mentioning, the production rates of **10H-8-MQL** accelerate sharply when the concentration of **4H-8-MQL** reaches the maximum, indicating that the **8-MQL** hydrogenation undergoes two steps: **8-MQL** → **4H-8-MQL** and **4H-8-MQL** → **10H-8-MQL**, and the second step is the rate-controlling step as stated previously.

In order to make an investigation on the catalyst degradation, the same catalyst was reused for 7 times hydrogenation of **8-MQL** at 160 °C and 7 MPa. The results have been displayed in Fig. 5c and d. Clearly, full hydrogenation of **8-MQL** was observed only in the first hydrogenation catalyzed by the fresh Ru/Al$_2$O$_3$. However, as expected, almost 100% of **4H-8-MQL** was obtained and very few **10H-8-MQL** was observed in the remaining cycles. In addition, the conversion rates of **8-MQL** gradually decreased with the increase of cycle times. This is probably because more effective active sites were covered by strong adsorption of **8-MQL**. Besides, the carbon deposits may be also responsible for the decrease of hydrogenation rate after recycling of the catalyst.[42] For the first cycle, the active sites of fresh Ru/Al$_2$O$_3$ are enough to catalyze **8-MQL** to form **4H-8-MQL** and **10H-8-MQL**. For the remaining cycles, the new **8-MQL** competes for effective active sites, some of which were probably gradually occupied by **8-MQL** with the increase of cycle numbers, thus hydrogenation rates decreased and **4H-8-MQL** was difficult to be further

Fig. 3 Hydrogenation of **8-MQL** at 160 °C and 7 MPa over Ru/Al$_2$O$_3$ (4 g **8-MQL**, 0.2 g Ru/Al$_2$O$_3$, 40 ml dioxane, 7 MPa H$_2$, 160 °C). After 180 min of reaction time another 0.1 g of fresh Ru/Al$_2$O$_3$ was introduced. (a) The hydrogen uptake curves for the whole process of **8-MQL** hydrogenation, (b) evolutions of **8-MQL** and the hydrogenated products during the whole hydrogenation process.

Table 1 Conversion and selectivity of 8-MQL hydrogenation with different catalyst dosage proportions at 160 °C and 7 MPa

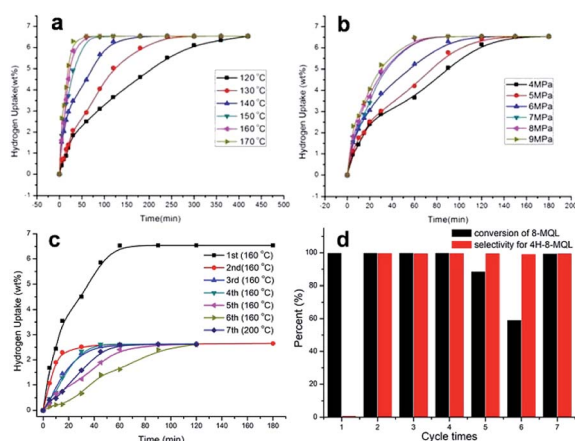| Test	Catalyst dosage proportion (wt%)	Reaction time (h)	Conversion (%)	Selectivity (%)	
				4H-8-MQL	10H-8-MQL
1	4	2	83.4	100	0
		5	100	99.1	0.9
2	5	2	91.3	100	0
		5	100	99.5	0.5
3	7	2	100	78.2	20.9
		5	100	23.1	76.9
4	10	2	100	0	100
		5	100	0	100
5	20	2	100	0	100
		5	100	0	100

hydrogenated to form **10H-8-MQL**. At the 7th cycle, the temperature was raised from 160 °C to 200 °C, which benefits the hydrogenation rate but still **10H-8-MQL** was rarely obtained.

Competitive adsorption shows a huge impact on the reaction rates in **8-MQL** hydrogenation. For quinoline substitutes, the adsorption of the reactant and its intermediate(s) was mainly through aromatic ring and nitrogen electron double. The solvents used in hydrogenation of quinoline derivatives play an important role in adsorption equilibrium.[39,43] Fig. 6 shows the concentration distributions of intermediates and products in **8-MQL** hydrogenation with different solvents. The reactions were conducted at 160 °C and 7 MPa with Ru/Al$_2$O$_3$ dosage proportion of 5 wt%. In the non-protic solvents, dioxane and toluene, almost complete conversion of **8-MQL** was found to form **4H-8-MQL** with only a trace of **10H-8-MQL** produced after 240 min. However, the conversion from **4H-8-MQL** to **10H-8-MQL** was observed in 120 min with ethanol as solvent in our experiment. A reason might be due to the hydrogen bonds formed between
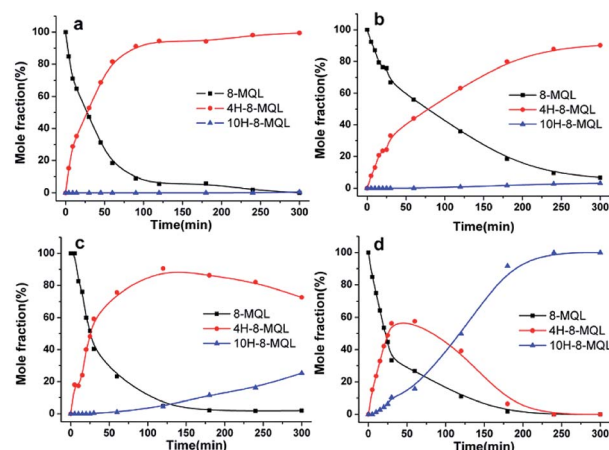
hydroxyl and N-heterocycle of **8-MQL**,[15] which weakens the strong adsorption of **8-MQL** on the active sites and benefits the adsorption of **4H-8-MQL**. For the base solvent, N,N-isopropylethylamine, the steric hindrance produced by the amine and its electronic interaction with the catalyst active sites probably avoided the strong adsorption of **8-MQL**,[43] thus 100% **10H-8-MQL** can be obtained in 240 min over Ru/Al$_2$O$_3$ in the presence of N,N-diisopropylethylamine (10 ml) and dioxane (30 ml) as solvent.

Adsorption of 8-MQL and 4H-8-MQL on Ru(0 0 1) surface

The geometries of **8-MQL** and **4H-8-MQL** were optimized by DFT calculations using Material Studio Dmol.³ The electronic charges of N-heteroatom in **8-MQL** and **4H-8-MQL** were −0.158 and −0.124 calculated by Hirshfeld method as displayed in Fig. 7a. The adsorption geometries of **8-MQL** and **4H-8MQL** were also optimized as shown in Fig. 7b. Kinds of possible adsorption geometries of **8-MQL** were investigated. It is found that the optimized adsorption geometry of **8-MQL** kept the two rings aligned parallel to the surface at a Ru–N distance of 2.150

Fig. 5 Time-dependent hydrogen uptake curves of **8-MQL** hydrogenation (a) at different temperatures (conditions: 4 g **8-MQL**, 0.4 g Ru/Al$_2$O$_3$, 40 ml dioxane, 7 MPa H$_2$) and (b) at different H$_2$ pressures (conditions: 4 g **8-MQL**, 0.4 g Ru/Al$_2$O$_3$, 40 ml dioxane, 160 °C) and (c) with the reused Ru/Al$_2$O$_3$ catalyst (conditions: 4 g **8-MQL**, 0.4 g Ru/Al$_2$O$_3$, 40 ml dioxane, 160 °C, 7 MPa H$_2$); (d) conversion and selectivity of **8-MQL** hydrogenation in 60 min for the 7 times cycles.

Fig. 6 The effects of solvents on hydrogenation of **8-MQL** over Ru/Al$_2$O$_3$: (a) dioxane (40 ml), (b) toluene (40 ml), (c) ethanol (40 ml), (d) N,N-diisopropylethylamine (10 ml) + dioxane (30 ml). General reaction conditions: 4 g **8-MQL**, 0.2 g Ru/Al$_2$O$_3$, 7 MPa H$_2$, 160 °C.
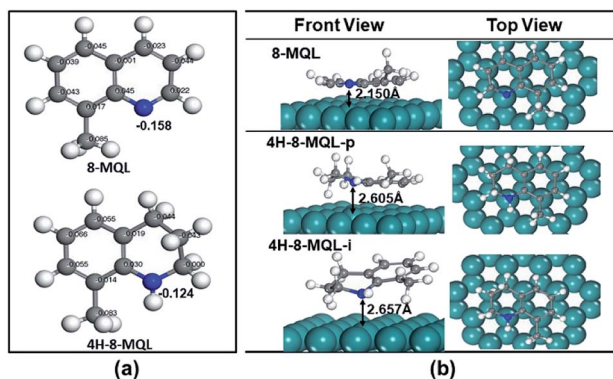
Fig. 7 (a) The atomic charges distributions of **8-MQL** and **4H-8-MQL**; (b) the optimized adsorption geometries of **8-MQL** and **4H-8-MQL** over Ru(0 0 1) surface with showing the distance between the N atom and the nearest Ru surface atom. Green: Ru atoms, blue: N, gray: C, white: H.

Å with the adsorption energy of 1.8 eV. Preferential hydrogenation of **8-MQL** occurs in N-heterocycle in the view of large amount of 1,2,3,4-**4H-8-MQL** formed in hydrogenation. It is can be explained by the strong coordination interaction of N atom to Ru surface. Two types of geometries of **4H-8-MQL** adsorbed on Ru(001) were optimized. Its aromatic ring aligned parallel to the surface was recorded as **4H-8-MQL**-p and the aromatic ring was positioned inclined to the Ru surface recorded as **4H-8-MQL**-i. The distance between N atom and the nearest Ru atom for **4H-8-MQL**-p and **4H-8-MQL**-i were 2.605 Å with the adsorption energy of 0.6 eV and 2.657 Å with the adsorption energy of 0.4 eV, respectively. Obviously, **4H-8-MQL**-p exhibited a stronger adsorption to **4H-8-MQL**-i. This suggests that the adsorption of **4H-8-MQL** was mainly *via* configuration **4H-8-MQL**-p, which can be attributed to the π-coordination of phenyl at Ru surface.[44]

Scheme 2 summarized the conversion and selectivity in hydrogenation of **4H-8-MQL** and **8-MQL** with reused catalysts. With more electronegativity of the N atom, basic **8-MQL** is easier to adsorb on the metal surface by coordination and occupy the acid sites on the support with higher adsorption energy. **4H-8-MQL** can be hydrogenated to form **10H-8-MQL** with reused Ru/Al$_2$O$_3$ in 3 cycles, indicating that **4H-8-MQL** was not responsible for poisoning the catalyst. For the process of **8-MQL** hydrogenation, the occupied acid sites on the supported by **8-MQL** prevent the **4H-8-MQL** from adsorbing and being active. Consequently, **10H-8-MQL** was rarely produced with limited catalyst active sites. Increase of the catalyst dosage proportion was benefit of the formation of **10H-8-MQL**. However, the new added **8-MQL** competes for effective active sites, some of which were probably gradually occupied by **8-MQL** with the increase of cycle numbers, thus very little **10H-8-MQL** was obtained in the remaining cycles. It is noted that the adsorption energies of the aromatic molecules are involved with the adsorption geometries, activated sites and adsorption sites. Nevertheless, the adsorption of QL substitutes benefits from the electronic charges of N atom, which leads to the strong interaction with the catalyst surface.

Experimental

Materials

8-MQL was provided from Alligator Reagent, which was further purified by vacuum distillation. Commercial 5 wt% Ru/Al$_2$O$_3$ catalyst was supplied by Shanxi Kaida Chemical Engineering Company Limited. Sinopharm Chemical Reagent Company Limited supplied 1,4-dioxane, ethanol and toluene. Energy Chemical Company provided *N,N*-diisopropylethylamine. All solvents and catalysts were used as received. Ultra-high purity of H$_2$ and Ar were provided by Sichuan Ally High-Tech Company. All liquid samples taken from reactors during experiments were regularly detected by Gas Chromatography and Mass Spectrometry (Agilent 7890/5975C, GCMS) to determine the composition. The samples diluted by hexane were carried by ultra-high purity He at a flow rate of 1.5 ml min^{-1} into the chromatographic column (HP-5, 30 m × 320 μm × 0.25 μm). The injection temperature was 300 °C and split ratio was 1 : 100. The oven temperature started at 90 °C, then increased to 220 °C by 12 °C min^{-1} subsequently and kept 220 °C for 1 min. Nuclear magnetic resonance (Bruker 400, NMR) was applied to determine the structure of **4H-8-MQL** produced in **8-MQL** hydrogenation.

Hydrogenation of 8-MQL and 4H-8-MQL

Hydrogenation process was carried out at a 600 ml stainless steel batch reactor (Parr 4568). After the reactants were loaded, the reactor was sealed and flushed with hydrogen to remove air for 4 times. Then the reactor was heated to the designed temperature and pressurized to the designed pressure. The pressure kept unchanged over the entire experiment by adding hydrogen continuously. The reaction time was recorded as zero when the magnetic stirring was started with a speed of 600 rpm. The liquid samples were taken periodically and analyzed by GCMS.

DFT calculations

The geometry configurations of **8-MQL** and **4H-8MQL** were optimized by the software of Material Studio DMol.³ The double numerical plus polarization (DNP) was applied to analyze valence electron orbitals.[45,46] Perdew–Wang-91 (PW91) was used to calculate nonlocal exchange and interrelation energies based on the generalized gradient approximation (GGA).[47] The charges of N-heteroatom in **8-MQL** and **4H-8-MQL** were calculated by Hirshfeld method.[48] The Ru(0 0 1) surface with a 5 × 5 supercell and three Ru layers with 20 Å vacuum region was built. The adsorption geometries of **8-MQL** and **4H-8-MQL** was optimized by stabilizing the last layer of Ru atoms in the supercell and relaxing the molecule on the top two layers of Ru(0 0 1). The adsorption energy was calculated by the Vienna *Ab initio* Simulation Package (VASP) according to the equation below:

$$E_{adsorption} = E_{surface} + E_{molecule} - E_{surface-molecule}$$

Scheme 2 Summary of catalyst cycles in hydrogenation of **4H-8-MQL** and **8-MQL** under designed conditions.

The $E_{surface}$, $E_{molecule}$ and $E_{surface-molecule}$ were the energy of the surface, the energy of absorbed molecule and the adsorption energy of the system. A plane wave basis set with a cutoff energy of 400 eV was used to solve the Kohn–Sham equation and the electron–ion interactions were described by the projector augmented wave (PAW) method.[49] The Brillouin zone was sampled within a $2 \times 2 \times 1$ Monkhorst–Pack k-point mesh. Electron smearing was employed by using the Methfessel–Paxton technique with a width of 0.2 eV to minimize the errors in the Hellmann–Feynman forces. Structural optimizations were performed until the total energy of the system was converged to less than 10^{-3} eV.

Conclusions

4H-QLs are formed as the main products in hydrogenation of QLs under mild conditions in general. This was explained mostly by the irreversible adsorption of QL and/or 4H-QL on the catalyst surface. The particular research on the adsorption behaviors of QLs and 4H-QLs have been rarely reported. In our work, it is demonstrated that **4H-8-MQL** is not responsible for the catalyst poisoning. The competitive adsorption behaviors of **8-MQL** and **4H-8-MQL** on Ru/Al$_2$O$_3$ was compared by a series of hydrogenation reactions and DFT calculations. The adsorption geometries and adsorption energies of **8-MQL** and **4H-8-MQL** were confirmed. It is found **8-MQL** is easier to adsorb on the

catalyst active sites by the interaction of N atom and Ru atoms compared with **4H-8-MQL**. Hydrogenation of **8-MQL** in mild conditions mainly generates **4H-8-MQL**. It is probably because of the strong adsorption of **8-MQL**, which occupies most of the active sites on the support and metal active sites. Fully hydrogenated product can be detected by increasing the catalyst dosage proportion of Ru/Al$_2$O$_3$. In addition, the production of **10H-8-MQL** can be promoted by introducing a protic solvent or Lewis base. The selectivity to **4H-8-MQL** or **10H-8-MQL** is related with the competitive adsorption between **8-MQL** and **4H-8-MQL**. Increasing the metal dispersion and the amount of acid sites on the supported is probably another way to benefit the formation of **10H-8-MQL** in **8-MQL** hydrogenation.

Conflicts of interest

There are no conflicts to declare.

Acknowledgements

Notes and references

1 F. Sotoodeh, B. J. M. Huber and K. J. Smith, *Int. J. Hydrogen Energy*, 2012, **37**, 2715–2722.

2 A. M. Maj, I. Suisse, C. Hardouin and F. Agbossou-Niedercorn, *Tetrahedron*, 2013, **69**, 9322–9328.

3 M. Campanati, M. Casagrande, I. Fagiolino, M. Lenarda, L. Storaro, M. Battagliarin and A. Vaccari, *J. Mol. Catal. A: Chem.*, 2002, **184**, 267–272.

4 T. Ben Issa, C. Ben Ali Hassine, H. Ghalla, H. Barhoumi and L. Benhamada, *J. Mol. Struct.*, 2018, **1162**, 71–80.

5 V. Sridharan, P. A. Suryavanshi and J. C. Menendez, *Chem. Rev.*, 2011, **111**, 7157–7259.

6 D. Ventura-Espinosa, A. Marza-Beltran and J. A. Mata, *Chem.–Eur. J.*, 2016, **22**, 17758–17766.

7 P. T. Aakko-Saksa, C. Cook, J. Kiviaho and T. Repo, *J. Power Sources*, 2018, **396**, 803–823.

8 Y. Wu, Z. Chen, W. C. Cheong, C. Zhang, L. Zheng, W. Yan, R. Yu, C. Chen and Y. Li, *Chem. Sci.*, 2019, **10**, 5345–5352.

9 C. H. Yang, X. Chen, H. Li, W. Wei, Z. Yang and J. Chang, *Chem. Commun.*, 2018, **54**, 8622–8625.

10 D. M. Zhu, H. B. Jiang, L. Zhang, X. L. Zheng, H. Y. Fu, M. L. Yuan, H. Chen and R. X. Li, *ChemCatChem*, 2014, **6**, 2954–2960.

11 X. Qiao, M. El-Shahat, B. Ullah, Z. Bao, H. Xing, L. Xiao, Q. Ren and Z. Zhang, *Tetrahedron Lett.*, 2017, **58**, 2050–2053.

12 M. G. Manas, L. S. Sharninghausen, E. Lin and R. H. Crabtree, *J. Organomet. Chem.*, 2015, **792**, 184–189.

13 P. Ryabchuk, A. Agapova, C. Kreyenschulte, H. Lund, H. Junge, K. Junge and M. Beller, *Chem. Commun.*, 2019, **55**, 4969–4972.

14 F. Fache and O. Piva, *Synlett*, 2004, 1294–1296, DOI: 10.1055/s-2004-825603.

15 H. Mao, C. Chen, X. Liao and B. Shi, *J. Mol. Catal. A: Chem.*, 2011, **341**, 51–56.

16 C. Wan, Y. An, F. Chen, D. Cheng, F. Wu and G. Xu, *Int. J. Hydrogen Energy*, 2013, **38**, 7065–7069.

17 M. Campanati, S. Franceschini, O. Piccolo and A. Vaccari, *New ways for the full hydrogenation of quinoline in mild conditions*, CRC Press-Taylor & Francis Group, Boca Raton, 2005.

18 M. M. Dell'Anna, V. F. Capodiferro, M. Mali, D. Manno, P. Cotugno, A. Monopoli and P. Mastrorilli, *Appl. Catal., A*, 2014, **481**, 89–95.

19 Y. Gong, P. Zhang, X. Xu, Y. Li, H. Li and Y. Wang, *J. Catal.*, 2013, **297**, 272–280.

20 B. Sun, D. Carnevale and G. Süss-Fink, *J. Organomet. Chem.*, 2016, **821**, 197–205.

21 X. Yu, R. Nie, H. Zhang, X. Lu, D. Zhou and Q. Xia, *Microporous Mesoporous Mater.*, 2018, **256**, 10–17.

22 H. Bernas, N. Kumar, A. Aho, R. Leino and D. Y. Murzin, *Catal. Commun.*, 2014, **56**, 41–44.

23 S. Zhang, Z. Xia, T. Ni, Z. Zhang, Y. Ma and Y. Qu, *J. Catal.*, 2018, **359**, 101–111.

24 F. Chen, A. E. Surkus, L. He, M. M. Pohl, J. Radnik, C. Topf, K. Junge and M. Beller, *J. Am. Chem. Soc.*, 2015, **137**, 11718–11724.

25 H. Y. Jiang, S. S. Zhang and B. Sun, *Catal. Lett.*, 2018, **148**, 1336–1344.

26 X. Yuan, N. Yan, C. Xiao, C. Li, Z. Fei, Z. Cai, Y. Kou and P. J. Dyson, *Green Chem.*, 2010, **12**, 228–233.

27 Y. Hu, Y. Yu, Z. Hou, H. Yang, B. Feng, H. Li, Y. Qiao, X. Wang, L. Hua, Z. Pan and X. Zhao, *Chem.–Asian J.*, 2010, **5**, 1178–1184.

28 Á. Vivancos, M. Beller and M. Albrecht, *ACS Catal.*, 2017, **8**, 17–21.

29 R. A. Sánchez-Delgado and E. González, *Polyhedron*, 1989, **8**, 1431–1436.

30 R. H. Fish, A. D. Thormodsen and G. A. Cremer, *J. Am. Chem. Soc.*, 1982, **104**, 5234–5237.

31 G. Zhu, K. Pang and G. Parkin, *J. Am. Chem. Soc.*, 2008, **130**, 1564–1565.

32 R. B. Xu, S. Chakraborty, H. M. Yuan and W. D. Jones, *ACS Catal.*, 2015, **5**, 6350–6354.

33 I. Sorribes, L. Liu, A. Doménech-Carbó and A. Corma, *ACS Catal.*, 2018, **8**, 4545–4557.

34 Z. Wei, Y. Chen, J. Wang, D. Su, M. Tang, S. Mao and Y. Wang, *ACS Catal.*, 2016, **6**, 5816–5822.

35 F. Martinez-Espinar, P. Blondeau, P. Nolis, B. Chaudret, C. Claver, S. Castillón and C. Godard, *J. Catal.*, 2017, **354**, 113–127.

36 Y. P. Sun, H. Y. Fu, D. l. Zhang, R.-X. Li, H. Chen and X.-J. Li, *Catal. Commun.*, 2010, **12**, 188–192.

37 L. M. Kustov, A. L. Tarasov and B. P. Tarasov, *Int. J. Hydrogen Energy*, 2013, **38**, 5713–5716.

38 R. M. Zhang, G. Y. Fan, C. Li, Y. Y. Wang, R. X. Li, H. Chen and X. J. Li, *Acta Phys.-Chim. Sin.*, 2008, **24**, 965–970.

39 M. C. M. Campanati, I. Fagiolino, M. Lenarda, L. Storaro, M. Battagliarin and A. Vaccari, *J. Mol. Catal. A: Chem.*, 2002, **184**, 6.

40 G. Y. Fan and J. Wu, *Catal. Commun.*, 2013, **31**, 81–85.

41 F. A. K. Bing Sun, A. Vallat and G. Süss-Fink, *Appl. Catal., A*, 2013, **467**, 5.

42 B. F. M. F. Williams, A. Jentys, C. Breitkopf, J. A. R. van Veen and J. A. Lercher, *J. Phys. Chem. C*, 2010, **114**, 10.

43 A. V. M. Campanati and O. Piccolo, *J. Mol. Catal. A: Chem.*, 2002, **179**, 6.

44 I. Favier, S. Massou, E. Teuma, K. Philippot, B. Chaudret and M. Gomez, *Chem. Commun.*, 2008, 3296–3298, DOI: 10.1039/b804402c.

45 F. W. Averill and D. E. Ellis, *J. Chem. Phys.*, 1973, **59**, 6412–6418.

46 A. D. Becke and R. M. Dickson, *J. Chem. Phys.*, 1988, **89**, 2993–2997.

47 A. D. Becke, *Int. J. Quantum Chem.*, 1985, **27**, 10.

48 X. Y. Zhou, C. Y. Rong, T. Lu and S. B. Liu, *Acta Phys.-Chim. Sin.*, 2014, **30**, 2055–2062.

49 G. Kresse and D. Joubert, *Phys. Rev. B: Condens. Matter Mater. Phys.*, 1999, **59**, 1758–1775.